SUPPLEMENTARY INFORMATION

Supplementary Figure 1

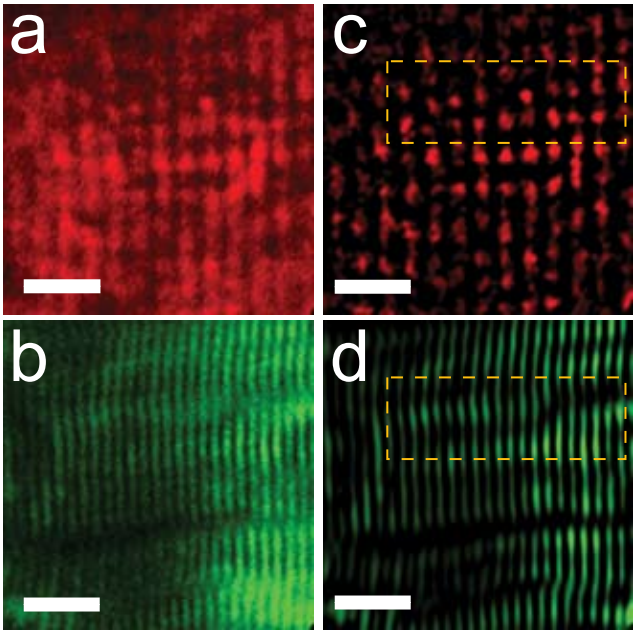

Supplementary Figure 1 | Static imaging of individual sarcomeres. a, Image of a single mouse muscle fiber in culture, acquired using epi-detection of two-photon excited autofluorescence. **b**, Image of the same fiber in a, acquired using trans-detection of second-harmonic generation (SHG). **c,d**, Band-pass filtered versions of a and b, highlighting sarcomeres. Yellow boxes indicate the regions of interest used to make Figures 2a,b.

Supplementary Video 1 | A three-dimensional stack of images acquired by second-harmonic microendoscopy from the lateral gastrocnemius muscle of a living mouse. A 1-mm-diameter microendoscope placed on top of the muscle was used to create an image stack extending 135 μm in depth and containing 270 images acquired at 0.5 μm increments. The imaging parameters and optical arrangement were the same as in all other animal imaging experiments (Methods). The white scale bar indicates 50 μm.

Supplementary Methods

***In vitro* imaging.** Single muscle fibers were prepared by enzymatic dissociation of tibialis anterior from C57bl/6 mice using a method modified from Carroll et al[31]. Tibialis anterior from a freshly sacrificed adult C57bl/6 mouse was incubated in 0.2% collagenase (Sigma, type IV) solution for 3-4 hours. After incubation, single fibers were obtained by trituration with a wide-mouth pipette, transferred to 90% Ringer's solution (in mM, 2.7 KCl, 1.2 KH_2PO_4, 0.5 $MgCl_2$, 138 NaCl, 8.1 $NaHPO_4$, 1.0 $CaCl_2$; pH 7.4) and 10% fetal bovine serum, and incubated for <1 day. The imaging system comprised a custom laser-scanning microscope equipped with a wavelength-tunable, ultrashort-pulsed Ti:sapphire laser (Spectra-Physics, Mai Tai) and a 40× water 0.80 NA objective (Olympus, LUMPLFL). 720-nm-illumination was used to generate autofluorescence that was collected in the epi-direction and filtered with BG40 colored glass (Schott). 920-nm-illumination was used to generate SHG that was collected in the trans-direction by an identical 40× water microscope objective and filtered by an ET460/50m filter (Chroma). In some experiments using SHG, the polarization of the laser light was varied with a half-wave plate to verify polarization dependence or to optimize signal intensity. Acquired images were four frame averages of 512 × 512 pixels using an 8 μs pixel dwell time. No translation or rotation of individual images was used to align the overlaid images of Fig. 2c.

Animal Imaging. All animal procedures were approved by the Stanford Institutional Animal Care and Use Committee. Adult C57bl/6 mice were anesthetized by injection of ketamine (0.13 mg/g) and xylazine (0.01 mg/g i.p.). The hindlimb was shaved and fixed

to a frame such that joint angles could be controlled. The imaging site was periodically irrigated with Ringer's solution. In experiments on sarcomere dynamics, we stimulated the muscle supra-maximally using a muscle stimulator (Medtronic, model 3128) with tungsten wires surrounding the proximal tibial nerve, which innervates the lateral gastrocnemius. We generally used either a 1-mm-diameter doublet microendoscope (Grintech, GmbH), composed of a 0.75 pitch Li-doped gradient refractive index (GRIN) relay lens of 0.2 NA coupled to a 0.22 pitch Ag-doped GRIN objective lens of 0.48 NA and 250-µm-working distance in water, or a stainless steel clad 350-µm-diameter doublet microendoscope (Grintech, GmbH), composed of a 1.75 pitch Li-doped GRIN relay lens of 0.2 NA coupled to a 0.15 pitch Ag-doped GRIN objective lens of 0.40 NA with a 300-µm-working distance in water. We performed laser line-scanning by first acquiring a reference image in two spatial dimensions and then choosing a linear path parallel to the long axis of the fiber for subsequent line-scanning.

Model of sarcomere length versus joint angle. The change in muscle-tendon length (dl^{mt}) with change ankle joint rotation angle ($d\theta$) was determined using:

$$\frac{dl^{mt}}{d\theta} = ma,$$

where ma is the moment arm of the muscle[32]. The moment arm and its variation with joint angle were determined by calculating the distance to the joint's center of rotation along the direction normal to the muscle's line of action. We calculated the change in muscle fiber length (dl^{m}) with change in ankle angle during passive motion by assuming that tendon stretch was negligible and thus:

$$\frac{dl^m}{d\theta} = ma(\cos\alpha),$$

where α is the pennation angle of the muscle fibers[33]. Once the change in muscle fiber length with ankle angle was computed, the change in sarcomere length (dl^s) with joint angle (Fig. 3a) was estimated using:

$$\frac{dl^s}{d\theta} = ma\cos\alpha\left(l_o^s / l_o^m\right)$$

where the optimal muscle fiber length (l_o^m) was determined by measuring the fiber length at the resting joint angle. The sarcomere length at the optimal fiber length (l_o^s) was assumed to be 2.8 μm.

Human Imaging. All human imaging procedures were performed in accordance with FDA guidelines for the protection of human subjects (21 CFR 50) and approved by the Stanford Institutional Review Board. Subjects' forearms were restrained in a brace and fixed to the microscope's vibration-isolation table. All optical components were identical to those used during animal studies. However, all components, including microendoscopes and mounting components, contacting or potentially contacting human subjects at the imaging site were sterilized by autoclaving. After insertion of the microendoscope, subjects were asked to flex and extend their fingers and changes in sarcomere length were monitored. Duration of testing was <60 minutes in all cases.

Data Analysis. Band-pass filtered images of sarcomeres were computed from raw images by applying an 11th-order Butterworth filter that acts as a band-pass for spatial periods between 1-5 μm. All analyzed images contained between 20 and 50 sarcomeres.

For each muscle fiber, average sarcomere length was determined along each of a series of parallel lines aligned with the axis of the fiber. We report the mean and s.e.m. of this collection of measurements. Determinations of accuracy in average sarcomere length measured along a single line used the 95% confidence interval generated by a nonlinear least-squares curve fitting algorithm (Trust-Region algorithm[34], nonlinear least-squares method[35]). All data analysis was done in Matlab (Mathworks).

Assessment of sarcomere visibility. The intensities of epi-detected SHG and autofluorescence signals are influenced by several wavelength-dependent processes, including attenuation of illumination in thick tissue, generation of signal photons at the focal plane, scattering of signal photons, and attenuation of signal photons within the detection pathway. Both the spatial arrangement and the contrast ratio between the maximum and minimum signal intensities observed within individual sarcomeres also influence sarcomere visibility (Fig. 2a-e). After exploring the illumination wavelength range of 720-980 nm using our tunable Ti:sapphire laser, we found that given this light source and the transmittance characteristics of our microscope, SHG imaging with illumination of ~920 nm was most effective at revealing sarcomeres *in vivo*. We do not claim 920 nm is the optimum excitation wavelength for imaging sarcomeres in thick muscle tissue, but rather that SHG imaging with 920-nm-illumination permits characterization of sarcomere lengths and dynamics in live subjects.

Potential measurement errors. To minimize chances of photo-damage during imaging we maintained incident laser illumination below 30 mW, a reported approximate

threshold for tissue damage[36]. We also monitored for any physical signs of damage in the tissue. If a component of a muscle fiber or its lateral inter-fiber connections were substantially damaged, one might expect to see punctate, local differences in sarcomere structure distinct from surrounding tissue. We did not observe such effects, but rather observed sarcomeres with relatively uniform and smoothly varying lengths. We also performed control studies in which we tested quantitatively for any differences in sarcomere lengths between paired measurements obtained just prior to and then immediately after insertion of the microendoscope into the muscle. Prior to insertion we measured sarcomere lengths in the unperturbed muscle using an air objective (Olympus, 20×, 0.4 NA, LMPlanFL). We then inserted a microendoscope into the same tissue site and measured sarcomere lengths again. Comparison of the paired data sets revealed that sarcomere length determinations were virtually identical under the two conditions, differing by only 3.8 ± 2.4% (mean ± s.d.; n = 45 measurement sites) and thereby precluding any substantial errors due to microendoscope insertion.

Another potential source of measurement error is parallax due to misalignment of the microendoscope's optical axis relative to the muscle fibers' transverse planes. However, a measurement error of just 1% would require a misalignment of over 8 deg, which was not observed in our three-dimensional data sets acquired with the microendoscope placed atop the muscle. In the mouse lateral gastrocnemius we found that muscle fibers were nearly parallel to the face of the microendoscope. From three-dimensional image stacks we measured an average misalignment of 3.3 ± 1.8 deg (mean ± s.d.; n = 37 measurements from 4 stacks acquired in 4 mice). Such consistent mechanical alignment

probably results in part due to pressure from the microendoscope on the muscle fibers. We conclude that in the lateral gastrocnemius measurement errors due to orientational misalignment are usually negligible. Similarly, misalignment errors seem likely to be minor in muscles in which the fibers lie parallel to the surface of the muscle, but perhaps less so in muscles in which the fibers vary significantly from this orientation.

Supplementary References

31. Carroll, S.L., Klein, M.G. & Schneider, M.F. Calcium transients in intact rat skeletal muscle fibers in agarose gel. *Am. J. Physiol.* **269**, C28-34 (1995).

32. An, K.N., Takahashi, K., Harrigan, T.P. & Chao, E.Y. Determination of muscle orientations and moment arms. *J. Biomech. Eng.* **106**, 280-282 (1984).

33. Zajac, F.E. Muscle and tendon: properties, models, scaling, and application to biomechanics and motor control. *Crit. Rev. Biomed. Eng.* **17**, 359-411 (1989).

34. Dennis, J.E. & Schnabel, R.B. *Numerical Methods for Unconstrained Optimization and Nonlinear Equations*. (Society for Industrial and Applied Mathematics, Philadelphia; 1996).

35. Bates, D.M. & Watts, D.G. *Nonlinear Regression Analysis and its Applications*. (Wiley, New York; 1988).

36. Konig, K., Becker, T.W., Fischer, P., Riemann, I. & Halbhuber, K.J. Pulse-length dependence of cellular response to intense near-infrared laser pulses in multiphoton microscopes. *Opt. Lett.* **24**, 113-115 (1999).